THE BELL SYSTEM TECHNICAL JOURNAL
Vol. 59, No. 2, February 1980
Printed in U.S.A

Design of Bubble Device Elements Employing Ion-Implanted Propagation Patterns

By T. J. NELSON, R. WOLFE, S. L. BLANK, P. I. BONYHARD, W. A. JOHNSON, B. J. ROMAN, and G. P. VELLA-COLEIRO

(Manuscript received September 4, 1979)

Experimental 8-μm period magnetic bubble devices have been made using 270/Ne/2E14 + 130/H_2/2E16 patterned implants on YSmLuCaGe-IG films previously implanted uniformly with 80/Ne/1E14. For subsequent alignments, the patterned implant was converted, in selected areas, into a relief pattern by phosphoric acid etching. A 2000 A.U. SiO_2 prespacer was deposited next, followed by the deposition and ion beam delineation of 500 A.U. of Permalloy for detection. A subsequent 2000 A.U. spacer was then deposited and patterned with via holes for electrical connection between the Permalloy and a 5000 A.U. Al-Cu layer which was deposited and patterned with plasma etching or ion beam milling. Final passivation and opening of contact windows were standard. All designs at 8-μm period were implemented with 2-μm or larger features. Novel ion-implanted propagation patterns are shown which accomplish merge, inside turns, and double period propagation.

A conventional hairpin shape was chosen for the generator, and the structure was placed in a cusp on the strong side of the major loop. Phase and current margins are presented. The minimum generator current varied with the starting anisotropy of the bubble film. The minimum current was about 100 mA in films with H_k around 1700 Oe, when the shallow implant was unpatterned. When the shallow implant was patterned, lower values were obtained.

An N-shaped transfer gate was studied. The design provides both a strong gradient, to separate the bubble from the implant boundary, and a locally lowered bias region to trap the bubble until the correct in-plane field orientation results in normal propagation. Phase and current margins are shown for transfer-out. A hairpin linking cusps on the two sides of a horizontal loop was found to transfer both ways with good current margins. This gate can be used as an active merge or to reverse the order in a block to overcome topological difficulties

in a G-type major-minor loop chip. Using the same idea, a transfer gate was designed which transferred through a write line to the bottom of the minor loops. Good phase and current margins were obtained.

A combination of a 2-μm wide implanted channel, a hairpin conductor, and a symmetrically placed Permalloy serpentine has been studied in a nondestructive read-out (NDRO) mode. It appears that the serpentine has too few turns for good averaging of Permalloy domain effects, as these detectors are noisy. An alternate design used a simple Permalloy bar entirely over implanted material. The straight detector produced better signal-to-noise appearance, although at a lower signal level and higher stretch current. Two straight bars were used in conjunction with the channel design. Both detector and "dummy" sense the stripped-out bubble in this case. Low noise and the best figure of merit $\delta V/V \sim 0.38$ percent were obtained in the destructive read-out (DRO) mode of operation. Good signals were also obtained from a straight Permalloy bar located over an unimplanted region, in the DRO mode, with a separated dummy. A valid chip organization for the DRO mode is offered.

Thus, all necessary functions have been demonstrated for the design of 8-μm period major-minor loop-organized bubble devices based on ion-implanted propagation. At least 20-Oe margins are shown for all functions at 40-Oe drive field.

I. INTRODUCTION

Recently, multiple implantation conditions,[1] single epitaxial layer composition,[2,3] and propagation pattern designs[4] have been demonstrated that should permit the fabrication of major-minor loop-organized bubble memory devices based on the use of ion-implanted propagation patterns (I2P2's).[5] The use of I2P2's at 8-μm period is expected to permit at least a factor of two increase in the minimum feature size, relative to Permalloy propagation patterns (3P's) of the same period, while reducing the coil power by a factor of two or more. The device components are not yet developed, however. Some early investigations of propagation[5] and of other components[6,7] have been reported, and a more complete account[8] of nucleate generator design has been given. In this paper, descriptions are given of components which provide insight into the design of large circuits based on ion-implanted propagation.

Experimental 8-μm period magnetic bubble devices have been made on YSmLuCaGe-IG films, as indicated schematically in Fig. 1. The damaged layer has a stronger overall in-plane preference when a combination of three implantations is used to produce a more uniform damage profile, and a thicker layer with planar magnetization. Because of this stronger preference, single epitaxial garnet films can be used

both for the implanted layer and for the bubble domain supporting layer. In the present work, the implant closest to the surface was usually not patterned, as discussed below. The measured material parameters specified for the films used in this study were:

$$h = 1.85 \pm 0.15,$$

$$sw = 1.75 \pm 0.10,$$

in microns, and the resulting collapse field was about 260 Oe prior to implantation. Approximately 1.5 μm of AZ1350J was used for the patterned implant stop. The implantation blackened the resist patterns and even cracked large unpatterned areas. While the implantation heated the wafer enough to flow the resist, it also hardened the resist so excellent pattern integrity was maintained. The resist shape after implantation is shown in Fig. 2.

For subsequent alignments, the patterned implant was converted, in selected areas, into a relief pattern by phosphoric acid etching. The layers that completed the device are illustrated in Fig. 3. The Permalloy was deposited at about 350°C, which took the place of (and was also the reason for) the anneal formerly used to stabilize the implant. A 2000-angstrom SiO_2 prespacer was deposited next, followed by the deposition and ion beam delineation of 500 angstroms of Permalloy for detection. A subsequent 2000-angstrom spacer was then deposited and patterned with via holes for electrical connection between the Permalloy and a 5000-angstrom Al-Cu layer, which was deposited and

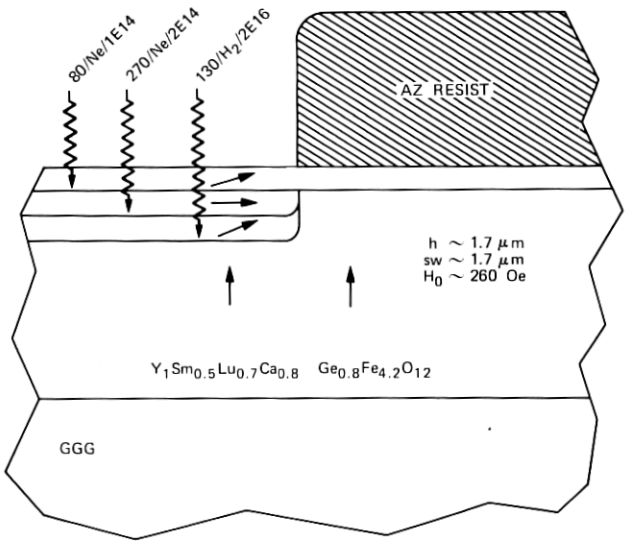

Fig. 1—Material composition and multiple implantation used for propagation at 8-μm period.

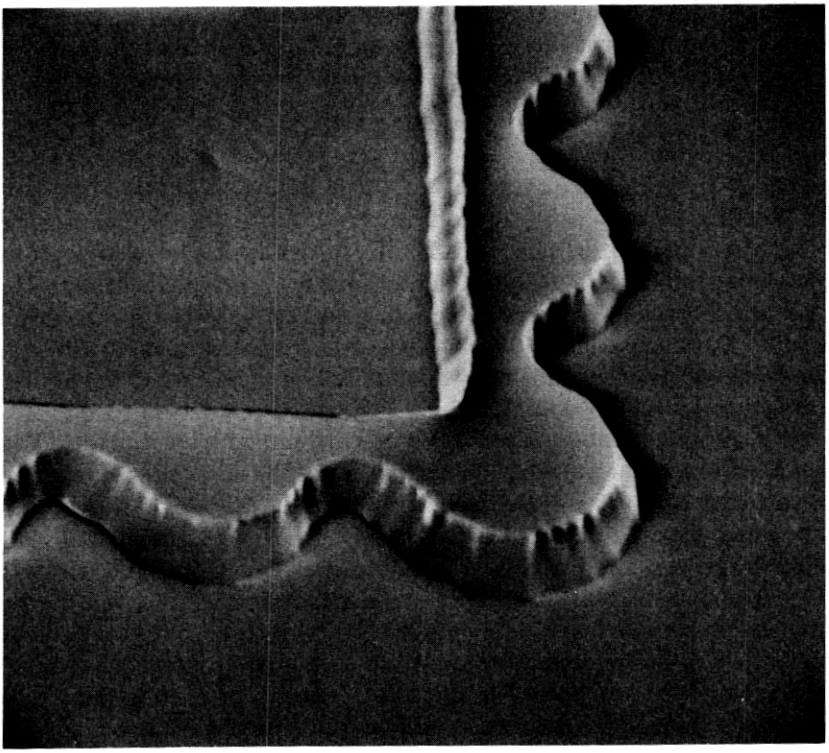

Fig. 2—SEM photograph at 45 degrees of approximately 1.5-μm AZ1350J photoresist after 270/Ne/2E14 cm^{-2} and 130/H_2/2E16 cm^{-2} implantation.

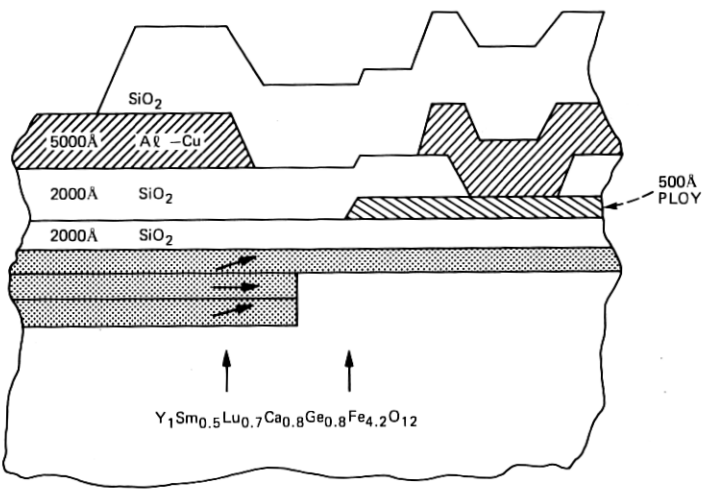

Fig. 3—Schematic cross section of oxide spacing, Permalloy, and Al-Cu levels in 8-μm period I2P2 devices.

patterned with plasma etching or ion beam milling. Final passivation and opening of contact windows were standard. The Al-Cu was processed after the Permalloy, but was heated to about 250°C by the passivation oxide deposition. In many cases, passivation was skipped, though, to improve turn-around time. No significant conductor edge crossing effects were observed in propagation in unpassivated wafers. There is evidence that the passivation lowered the generator current, which may point to stress in the Al-Cu. The electrical contact established in the via holes was sometimes faulty, even though a light "clean-up" ion milling step was done just before the Al-Cu deposition. All designs at 8-μm period were implemented with 2 μm or larger features. The coding of all mask levels used 0.5-μm EBES address steps.

II. PROPAGATION CONVENTIONS

The minor loop orientation was chosen as indicated in Fig. 4. It will be noticed that all turns shown are counterclockwise, for a counterclockwise rotating field. They are defined to be forward turns. These choices ensured the best overall propagation margins available. The overlap bias field margins shown in Fig. 5 were determined, at high bias by the roof-topped major loop[9] and at low bias by interaction between minor loops. These and all other data presented in this paper were taken at 50-kHz rotating field frequency. Unless otherwise noted, the rotating field intensity was 40 Oe with no in-plane dc offset field. The start-stop direction provided for the stabilization of the information bubbles at rest. This direction is referred to as 0 degrees. The bubbles in the minor loops came to rest in cusps, except for the one bubble in each loop which stopped at the $[2\bar{1}\bar{1}]$ end. These bubbles appeared to be stabilized by their symmetry preferred rest positions. The start-stop margins shown in Fig. 6 were taken by multiple rotating field bursts such that the bubbles stopped 10 times in each position in the loops for about 130 μs, and finally stopped long enough to be observed. As can be seen, an offset field $\geq$ 2 Oe is indicated for stabilization of the major loop. With few exceptions, the device components described below were operated in such a way that bubbles were propagated along a horizontal track past opposing minor loops spaced as shown in Fig. 4. Therefore, the interaction with the minor loops generally determined the low bias field margin. Consequently, although most of the results to be reported were obtained with different wafers, the low bias margin can be used as a reference value good for all.

III. SPECIAL-PURPOSE PROPAGATION (BASED ON CRYSTAL SYMMETRY)

Bubbles on separate tracks can be merged, with proper circuit orientation. The design shown in Fig. 7 consists of two horizontal 9-

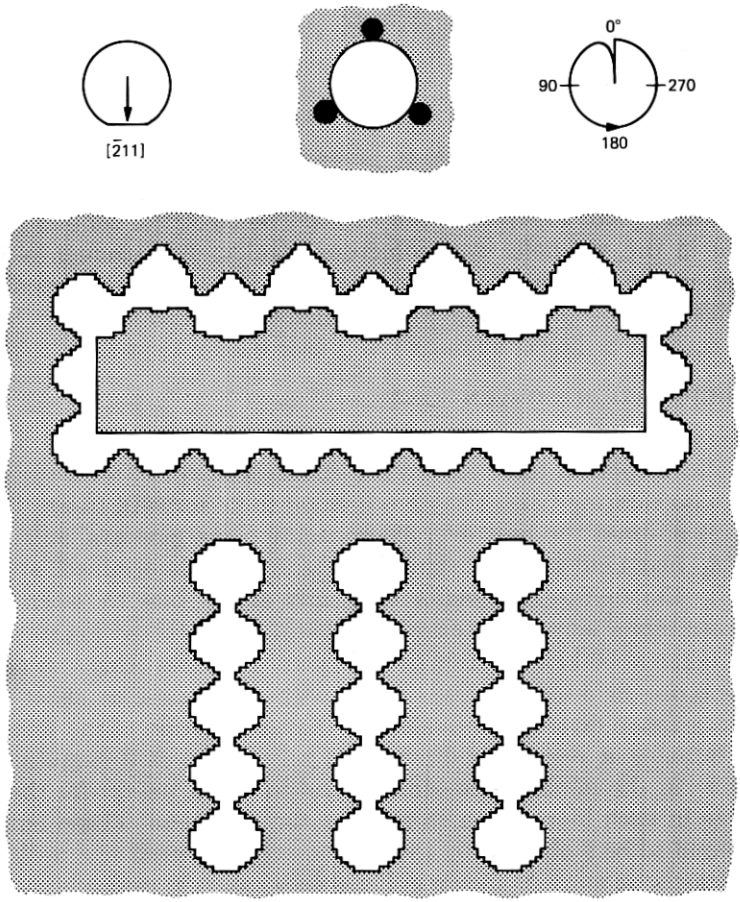

Fig. 4—Orientation and relative placement of major and minor propagation paths in 8-μm period I2P2 devices. The "roof-top" pattern replaces the weak side of the major loop.

step propagate loops situated as close as 2 μm apart. Actually, a series with gaps increasing in 1-μm steps was prepared. The gap, when small enough, had the remarkable property that it behaved like a cusp, when encountered by bubbles on the strong side. Bubbles approaching the gap from the weak side propagated through as though the adjacent loop were not present. Bitter fluid observations showed that charged wall motion proceeded smoothly from the weak side through the gap, but the motion was discontinuous going the other way. The bias field vs drive field intensity plot shown in Fig. 8 reproduces essentially the full margins of ordinary horizontal loops. The margins were taken by reversing the direction of propagation on alternate rotating field bursts. By this means, the bubbles appeared alternately on the two loops, and

both aspects of the merge were included in the margins. The merge function was significantly degraded in the case of the 3-μm gap. The weak side of any horizontal loop would be "roof-topped" in a practical device, and would therefore give wider margins than obtained here.

The inside-out loop design shown in Fig. 9 has been found to propagate well in some cases, as shown by the bias field vs drive field margins shown in Fig. 10. This type of loop has given inconsistent

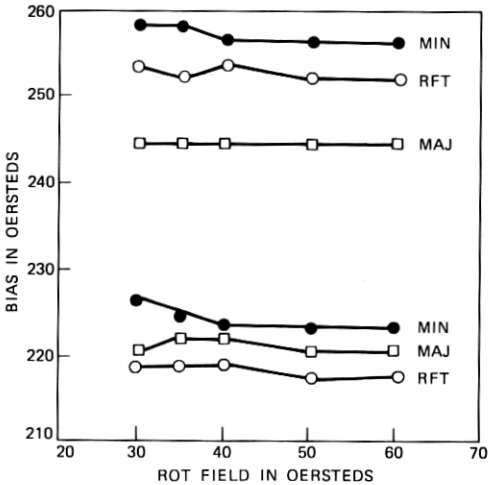

Fig. 5—Bias field margins vs drive field intensity for propagation structures in 8-μm period I2P2 bubble devices operated at 50 kHz. The roof-topped loop had no minor loops nearby to limit its low bias margin.

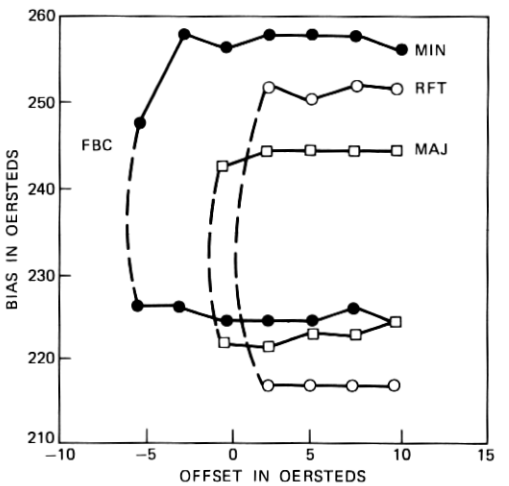

Fig. 6—Bias field margins vs offset field at 40-Oe drive field intensity for propagation structures in 8-μm period I2P2 devices.

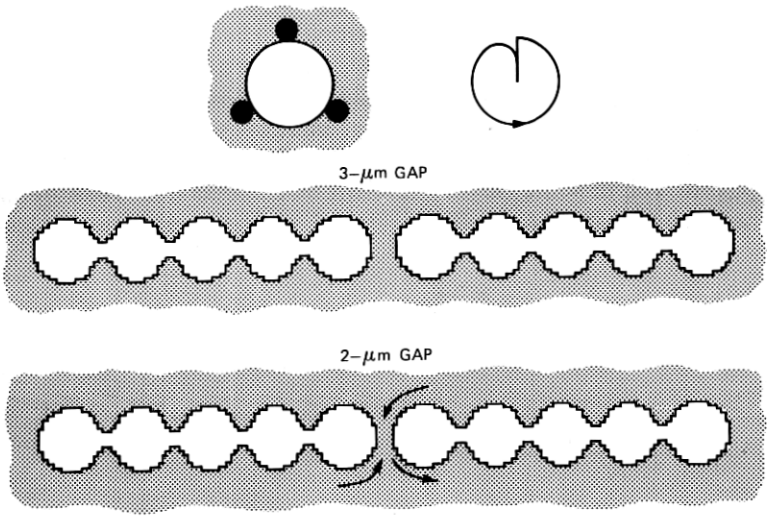

Fig. 7—Merge realized by 2-μm gap between horizontal propagation patterns. The gap is treated as a cusp by the bubbles entering on the strong (bottom) side and as a passage for bubbles propagating on the weak (top) side.

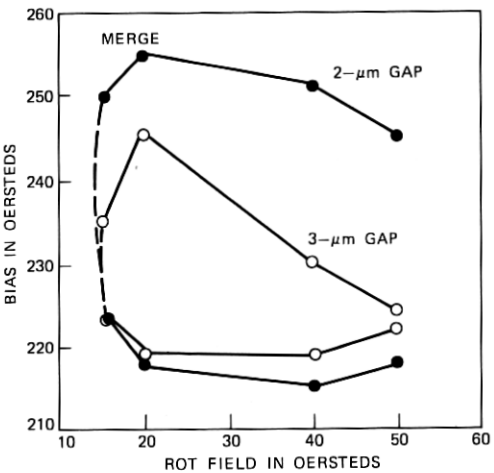

Fig. 8—Bias field margins vs rotating field intensity for alternating propagation directions (the bubbles pass from loop to loop on alternate bursts).

results in the past, however. It was found that 120°C baking of the implant photoresist, which sometimes occurred prior to implantation, affected the edges of the features significantly. Note that the ordinary propagation patterns shown in Fig. 4 continued to work well. The 180-degree backward turns can be used to form minor loops, as shown for testing, or can be combined with 90-degree forward turns to solve layout problems.

It was pointed out by Lin[10] that it might be advantageous in ion-implanted propagate circuits to have the capability of enlarging the period by a factor of two. For example, 2λ propagation on the major loop between minor loops doubles the data rate and reduces the maximum access time as well. The design shown in Fig. 11 retains the normal cusp, but stretches out the peak over the intervening distance. The bias field margins shown in Fig. 12 are satisfactory, although this design too was found to be sensitive to the treatment of the implant photoresist. Propagation back and forth on the strong side was tested

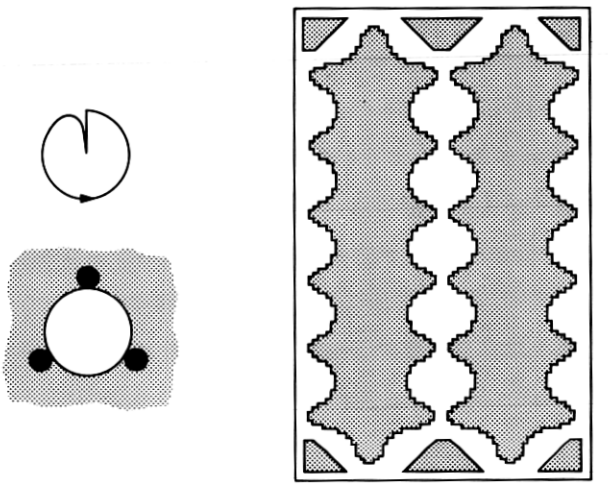

Fig. 9—Inside-out propagation loop design. The turns can be used individually to help solve layout problems or together to form a minor loop.

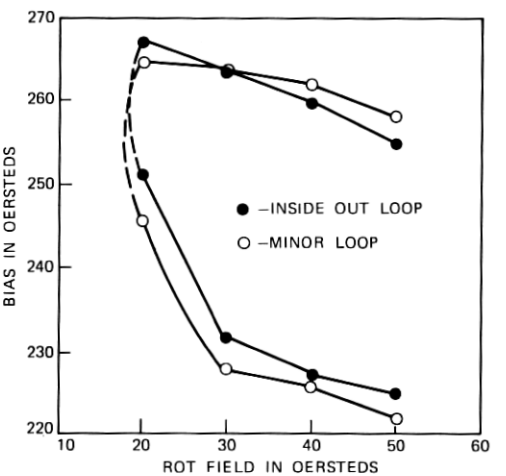

Fig. 10—Bias field margins vs drive field intensity for 8-μm period inside-out loop.

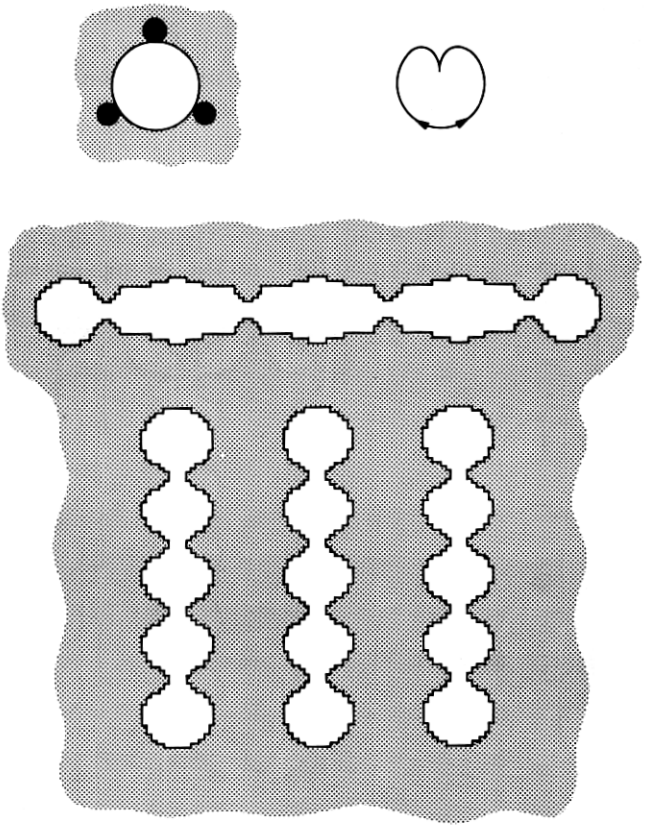

Fig. 11—Horizontal propagate loop in which the cusps are spaced by 2λ.

here, and is shown along with the same type of propagation in a minor loop for comparison.

IV. GENERATION

The design and orientation of the generator used in the present work is shown in Fig. 13. Its design is not importantly different from those used with Permalloy propagation patterns. The orientation, however, was determined by the tendency of the cusps on the strong side of the horizontal loop to nucleate more readily. The bias field margins for the generator on a particular garnet film are shown in Fig. 14 as functions of phase and current. These margins are composite to the extent that the bubbles were propagated past some minor loops, as shown in Fig. 4, before being stopped for observation. It will be noticed that the minimum nucleate current depends rather more on bias than would be the case with Permalloy propagation patterns. The margins

saturate at the propagation limit for the strong side of the horizontal loop. Increased current was permitted, but the phase margins began to constrict again at 200 mA.

The minimum generator current at low bias has also been found to vary from device to device. The values shown in Fig. 15 were obtained near the minimum bias at which generation and propagation on the strong side of the major loop, past the minor loops, could be achieved. The anisotropy field of each chip was measured by a microwave spin resonance technique. Obviously, the nucleation current must be held above a practical minimum, say, about 100 mA, to permit other control functions to be free of restrictive upper limits due to spurious nucleation. Evidently, this will require a minimum of about 1700 Oe in the anisotropy field H_K. Some of the first samples were implanted in the way previously reported[4] with all three implants patterned. However,

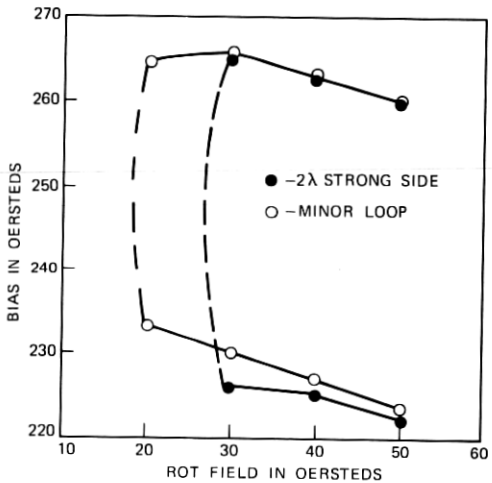

Fig. 12—Bias field margins vs drive field intensity for strong side of 2λ propagate loop.

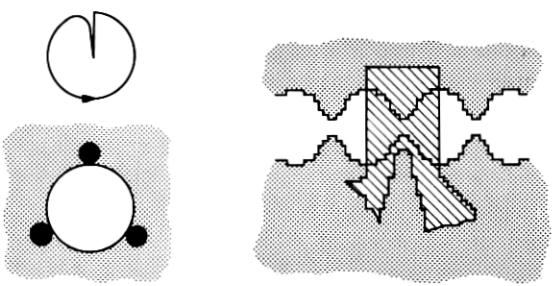

Fig. 13—Al-Cu hairpin generator placed in a cusp of the strong side of a horizontal ion-implanted propagation path.

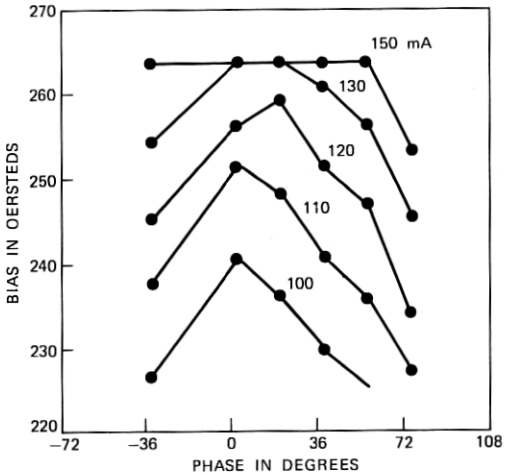

Fig. 14—Bias field margins vs phase and current for nucleate generator in I2P2.

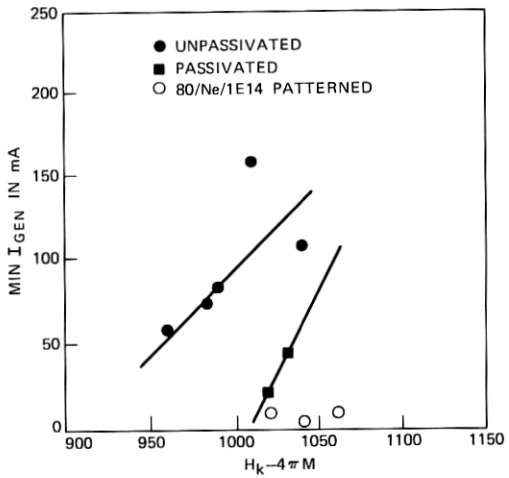

Fig. 15—Minimum generator current vs measured anisotropy field in I2P2 test devices.

as some of the experimental designs envisioned moving bubbles into the unimplanted region, certain wafers were implanted with the shallow 80/Ne/1E14 dose first, as though for a hard bubble suppression implant, before the photoresist pattern was applied. As it happened, the nucleation current was very low except with the wafers on which the shallow implant was unpatterned. All the other data in this paper were obtained on samples in which the shallow implant was not patterned. We believe that the effective step in bubble film thickness at the implant edge was reduced by this technique, while the implant thickness itself was unaffected.

V. TRANSFER GATE DESIGN

Various attempts at bi-directional transfer gate design have been made. Jouve[11] has favored a hairpin conductor shape, while Lin et al[6,7] proposed a straight wide conductor stripe. We found that hairpin designs did not work unless the conductor was pulsed hard enough to stretch the bubble between the minor loop and the major loop. The wide straight conductors tried tended to collapse bubbles rather than to transfer them, perhaps because of the large separation between the major and minor loops. Evidently, a strong bias field gradient is required, to separate the bubble from the implant edge, coupled with a favorable bias field environment. A design generated from this information resulted in a notched wide conductor that looks like the letter "N." We also found it feasible to transport bubbles through nominally unimplanted areas, which led to various useful functions.

VI. N-GATE

In the present work, the design shown in Fig. 16 has produced the best results to date, for transfer-out. The design is intended to provide a bias field gradient, to separate the bubble from the implant edge. At the same time, local lowering of the bias field, where the current circulates around the notches, is supposed to stabilize the bubble position. Also the design attempts to minimize the resistance per gate. In transfer-out, the bubble went directly from the end of the minor loop, which is a preferred position, to the cusp on the major loop. The current margins shown in Fig. 17 were obtained by using a pulse 72 degrees wide, starting at −54 degrees. The gate was pulsed on alternate cycles, so that in the first pass, or trip around the minor loop, the bubble experienced the pulse from positions adjacent to the gate. Collapse of the bubble in such neighboring positions prevented the bias margins from extending to higher currents at high bias. These data were obtained by transferring in at a fixed bias and transferring

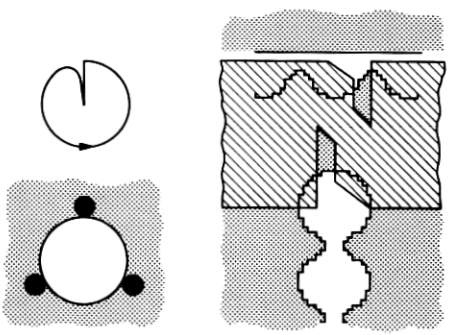

Fig. 16—N-shaped transfer gate design which provides both a gradient at the implant boundary to move the bubble and a local lowering of the bias field to trap it.

out at variable bias. A two-level pulse was used for transfer-in, starting with a high current for about 36 degrees followed by a lower current for about half a cycle. While good bias margins were sometimes achieved for transfer-in, acceptable current margins were not achieved. The tranfer-out phase margins are shown in Fig. 18.

VII. IMPLANT-BOUNDARY GATE

Interesting results were obtained with the design shown in Fig. 19. Here a current loop passes through the major loop, the original idea being to stretch the bubble from one side to the other. If the two ends of the strip could propagate independently, then eventually it would be possible to separate them by a subsequent cut pulse. While this was not achieved, after the bubble was stretched through the "unimplanted" region, which is only 2 μm wide, the originating end pulled out of the cusp, when this cusp became repulsive. Thus a transfer

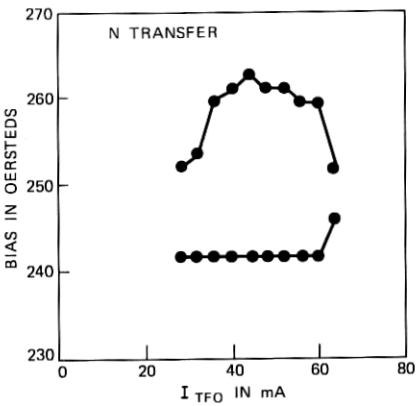

Fig. 17—Bias field vs current margins for transfer-out in N-type design on I2P2, with fixed optimal phase.

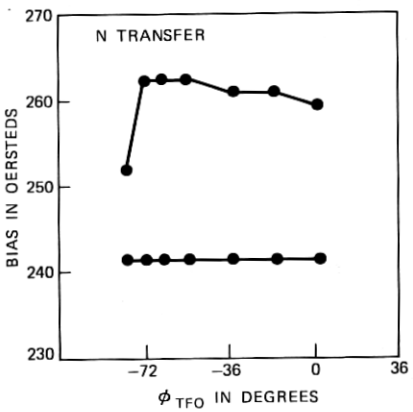

Fig. 18—Bias field vs phase margins for transfer-out in N-type design on I2P2.

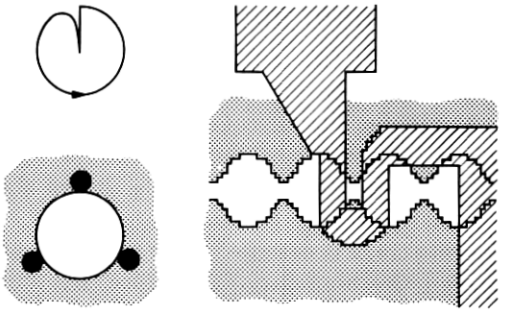

Fig. 19—Hairpin conductor loop linking the two sides of a horizontal loop and used for transfer through the unimplanted material.

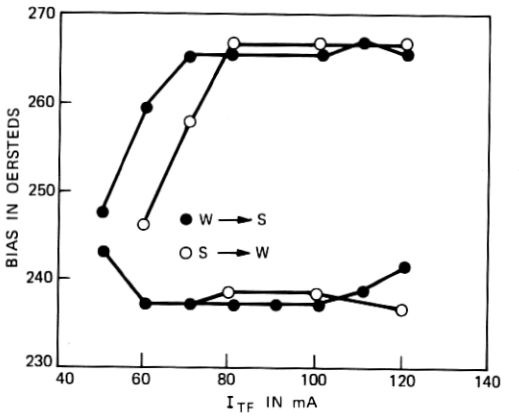

Fig. 20—Bias field vs current margins for transfer through unimplanted region of a horizontal loop.

action was achieved. The current margins for transfer both ways are shown in Fig. 20. In each case, the transfer pulse was 72 degrees long and terminated at the time that the cusp from which the bubble started had become repulsive. It is clear that the margins saturate at the propagation limit for this un-roof-topped horizontal loop. Evidently this gate might provide bidirectional transfer in a major-minor loop chip based on the inside-out propagation loop shown in Fig. 9. The margins of Fig. 20 do not include the effects the transfer pulses have on bubbles in adjacent cycles, however.

VIII. WRITE LINE TRANSFER

The use of separate read and write lines for the major-minor organization would eliminate the need for bidirectional transfer gates. Also, better performance might be expected from gate designs specialized for transfer in one direction. Since ion-implanted tracks only propagate bubbles on the implanted side of the boundary, however, it is not obvious how to propagate data taken from the read line into position

for transfer at the write line without reversing the order of the data with respect to the loops. The discovery that the unimplanted region could be tranversed, as described above, solved the topological aspect of the problem. The write line transfer gate design shown in Fig. 21 was operated similarly to the implant-boundary gate. The opposite side of the propagate track is designed to be repulsive, after the bubble is stripped through the boundary. Therefore, the bubble contracts again to the attractive position at the end of the minor loop. A 5-Oe offset field, added to the 40-Oe rotating field in the start-stop direction, improved the high bias limit. The bias field margins are composite functionally in the sense that bubbles were generated, propagated along the "snake" pattern, transferred into the minor loop, propagated around the minor loop, transferred out at the N-gate, and finally stopped for observation on the read line. The N-transfer on this device required higher current than the one described above and therefore did not have as good margins when the effect of neighboring positions was included. The implant photoresist in this batch of devices was subject to the 120°C bake mentioned above, which may be a problem. Bias vs current margins are shown in Fig. 22, for a 36-degree pulse turned on at 108 degrees. The phase margins are shown in Fig. 23. Inasmuch as this write-line transfer now appears to be superior to the N-gate, it will be desirable to further optimize the read line transfer for transfer-out only.

IX. DETECTION

So far, there is no analog for the chevron stretcher-detector in ion-implanted propagation patterns. Consequently, we examined designs that use an active conductor loop[12,13] to amplify the bubble flux for detection. Obviously, this method of detection will result in a signal-speed trade-off determined primarily by the saturation wall velocity. It should also be possible, in principle, to stop the rotating field (with

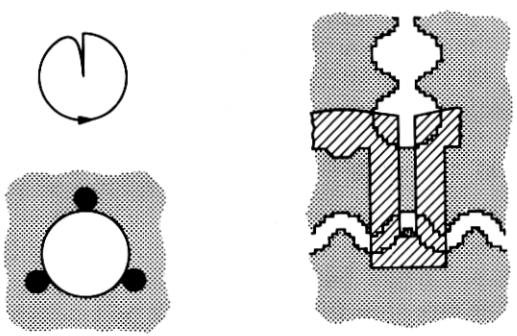

Fig. 21—Write line transfer gate in which bubbles pass through nominally unimplanted material.

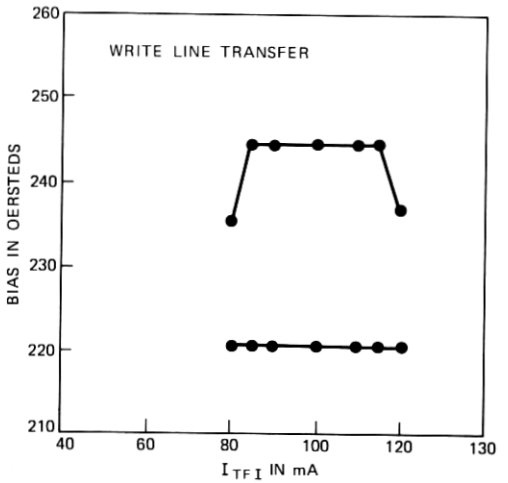

Fig. 22—Bias field margins vs current for write line transfer, with fixed optimal phase.

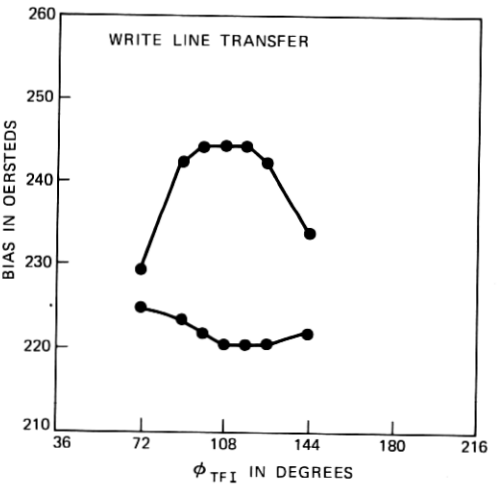

Fig. 23—Bias field margins vs phase for the write line transfer, at 40-Oe rotating field with a 5-Oe offset.

or without a holding value) to detect, with sufficient time allowed for expansion. In such a case, the data rate may be reduced, but the access time is not otherwise affected. This technique has not been resorted to in the present work. The approach we have attempted restricts the stretching to less than about 100 μm, and uses thinner Permalloy to increase the signal (and source impedance). The Permalloy thickness has been fixed at 500 angstroms in the present work, almost an order of magnitude less than the normal thickness for 3P's, which use the same Permalloy level for detection and propagation. The available

signal is not increased by a factor of 10, however, as the unreduced dc current would overheat the thinner Permalloy. Actually scaling the current to maintain constant power per square as the Permalloy thickness varies leads to a square-root improvement in signal level as the thickness is reduced. Figure 24 shows how the powered detector resistance varies with current. We infer that the temperature rise reaches 10°C at about 3 mA and consequently have used 2.5 mA in the present work. Generally, at this stage of the development it has been found easier to collapse the strip domain, after expansion and detection, than to de-expand to a bubble and return the bubble to a definite position on a propagate track. Destructive read-out (DRO) was expected to be primarily useful for characterization of the other functions, using electronic testing methods. Nondestructive read-out (NDRO) has been actively pursued, and two designs are discussed below.

X. CHANNEL-MEANDER DETECTOR

The structure shown in Fig. 25 has been operated in a nondestructive read-out (NDRO) mode. The conductor hairpin straddles a vertical 2-μm wide, ion-implanted channel. Due to the effect of the two edges, the strip-out (and collapse) fields are raised in the channel. The meandering Permalloy pattern was symmetrically placed astride the channel. Thus, all three levels contributed somewhat to the stretching of the bubble, but only the reversed polarity pulse destretched it. Still, the operational frequency limit would probably be imposed by stretching as destretching or collapsing have been obtained with shorter and

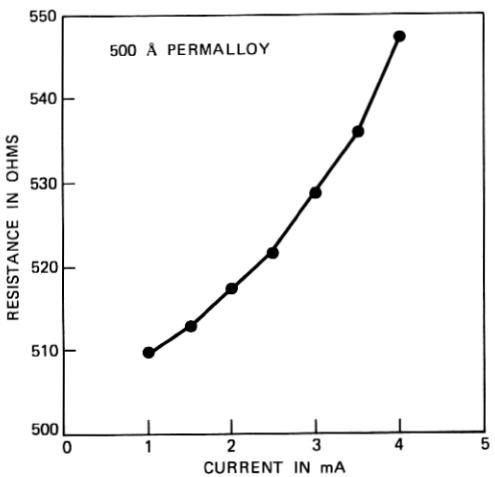

Fig. 24—In-circuit dc resistance vs bias current for 500 angstrom Permalloy detector. The increase in resistance indicates heating of the Permalloy.

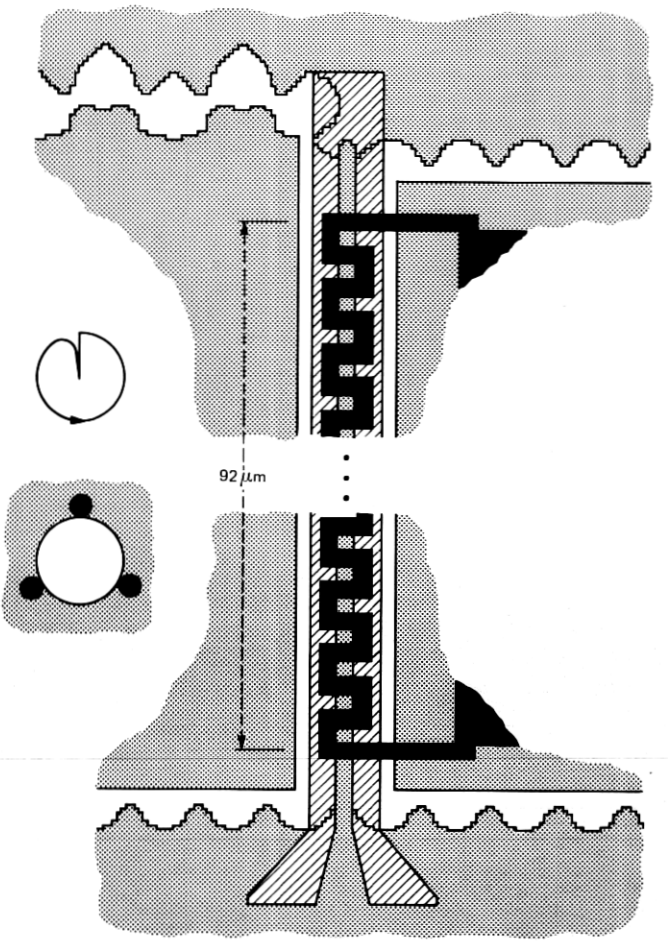

Fig. 25—Channel detector with extra cusp for controlling bubble after single-cycle stretch and destretch. Bubbles enter from bottom left and are stretched by the combined action of the implanted channel, the Permalloy, and a current pulse. A reverse pulse destretches the bubble and deposits it in the extra cusp at the top of the channel.

lower current pulses. The domain was carried by a current pulse to a position adjacent to the cusp at the top of the channel when that cusp became attractive. The reverse polarity pulse constricted the strip elsewhere, but enhanced the cusp position. As shown in Fig. 26, the minimum current for destretch was about 50 mA, while higher values for the stretch pulse may be needed. The output waveform is shown in Fig. 27. A differential pre-amplifier with a gain of 10 was used. The difference between the zero signal (more intense, as there were fewer ones) and the one signal was about 2 mV. An inverted signal is displayed, i.e., the presence of a bubble raises the detector's resistance.

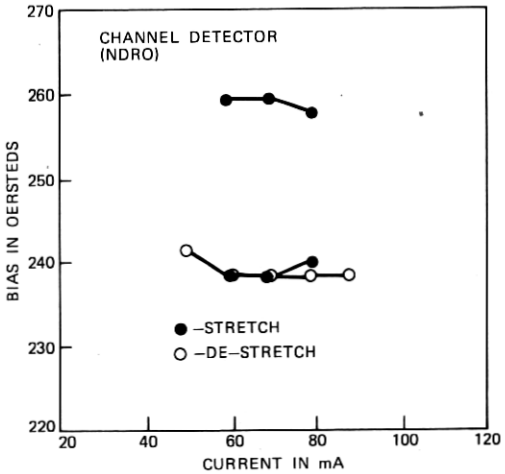

Fig. 26—Bias field margins vs current for stretch and destretch pulses in NDRO channel detector.

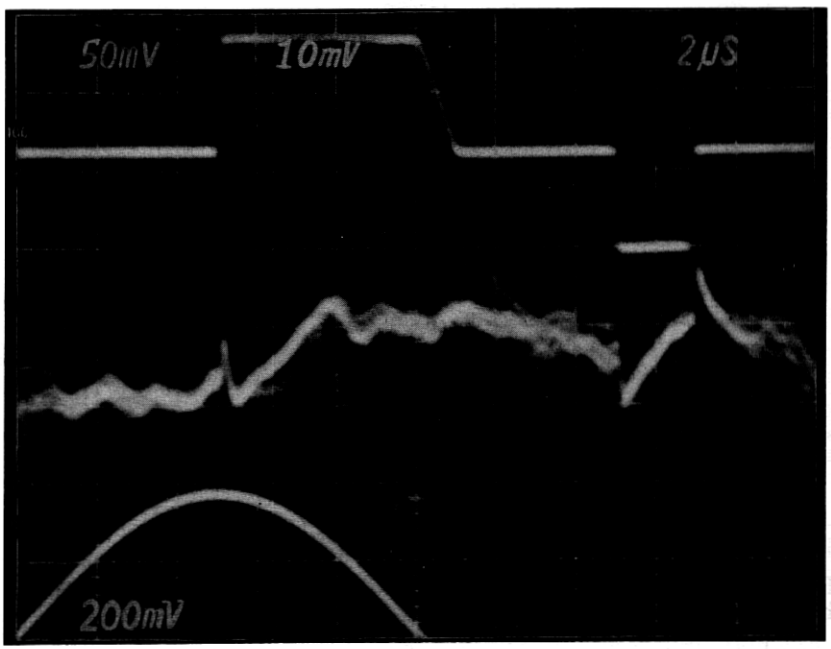

Fig. 27—Superimposed zero and one output waveforms of NDRO channel detector at 2.5 mA and 40-Oe drive field with 5-Oe offset.

The detector resistance was 430 ohms so the $(\delta V/V)$ figure of merit obtained was 0.19 percent. Also shown in Fig. 27 are the stretch conductor current waveform, at 1 mV/mA, and a representation of the x-coil current waveform (its peak defines 0°). The drive field was 40

Oe, with 5-Oe offset. The output was noisy, or not entirely reproducible from cycle to cycle. This noise is probably due to the small number of features (and correspondingly fewer domains) of the Permalloy design. Thick Permalloy detectors, by contrast, have about an order of magnitude more features.

XI. IMPLANTED-BAR DETECTOR

An alternate design, which reduced the geometrical intricacies, is shown in Fig. 28. This detector Permalloy is placed over the implanted region. The simple Permalloy bar had lower resistance, of course, but also produced a lower figure of merit. On the other hand, the signal was found to be more reproducible from cycle to cycle. The bias field vs current margins are shown in Fig. 29 and the output in Fig. 30. This detector was implemented in an isolated vertical loop, and therefore

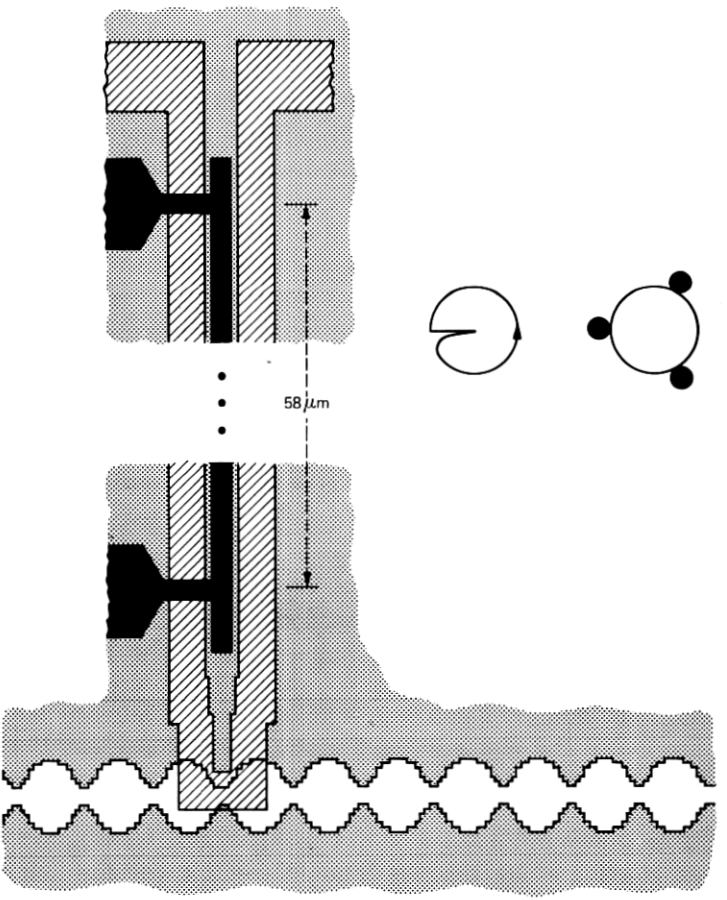

Fig. 28—Straight-bar detector design using cusp in vertical propagate track to re-trap the destretched bubble.

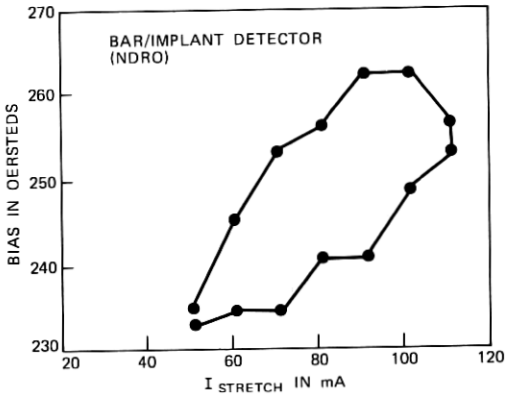

Fig. 29—Bias field margins vs stretch current for straight-bar NDRO detector.

its low bias margin extends below the value of useful propagation in a major-minor loop arrangement. The 0.8-mV signal at 2.5 mA into 235 ohms leads to a figure of merit of 0.13 percent. The small signal was nevertheless detectable electronically at 55-Oe rotating field intensity. No offset field was used. The output displayed is not inverted so the presence of a bubble lowers the detector resistance near 0°. This magnetoresistive response is understood to be caused by increased magnetization in the hard direction at the time that the bar switches. A remarkable feature of this design, wherein the Permalloy is entirely placed over implanted material, is that the destretching function is free; that is, in the bias range of interest the strip collapses back to a bubble in the cusp even at low bias. The interaction of bubbles or strips with the Permalloy over the implanted material was observed to be unexpectedly weak. Evidently, this can be interpreted as resulting from a large effective spacing because of the thick implanted layer.

XII. CHANNEL-BAR DETECTOR

A variation of the channel detector design is shown in Fig. 31. Two straight Permalloy bars were placed astride the ion-implanted channel, preserving the symmetry which helps to keep the bubble in the channel. One bar acts as the detector, while the other acts as the reference, or "dummy," detector. The strip's field adds to the drive field on one of the elements and subtracts on the other. Both the dummy and the detector contribute to the differential signal. The bias field margins for this detector operated in the DRO mode are given in Fig. 32. As shown in Fig. 33, a 50-mA collapse pulse was applied for 36 degrees, starting at 180 degrees. The differential waveform shown in Fig. 33 was obtained with the lefthand element uninverted (still at a gain of 10). The fainter trace was due to bubbles, as there were more

cycles containing zeros. The dip in the zero trace is magnetoresistive, as it changes sign when the stretch pulse is delayed by half a cycle. By displaying the signals due to both bars independently, it was verified that both contribute about equally. The drive field was 40 Oe and a 5-Oe offset along 0 degrees was applied. The 3-mV signal was obtained with 2.5 mA into 320 ohms so the figure of merit was 0.38 percent.

XIII. UNIMPLANTED-BAR DETECTOR

A version of the straight-bar detector which was suggested by the transfer gate designs that use the unimplanted region is shown in Fig. 34. It was possible to transfer and stretch at the same time, as the current needed was in the same range for both effects. The stretch current was probably reduced for the same reason that the signal was increased: the effective spacing between bubble and Permalloy was reduced by removing the deep implants from under the Permalloy. The stretch and collapse current margins observed are shown in Fig. 35, while a typical output waveform is shown in Fig. 36. This detector was operated in the DRO mode. A collapse pulse of about 75 mA was typically applied, starting at 180 degrees. The detector resistance was reduced by the presence of the domain at the time the magnetization

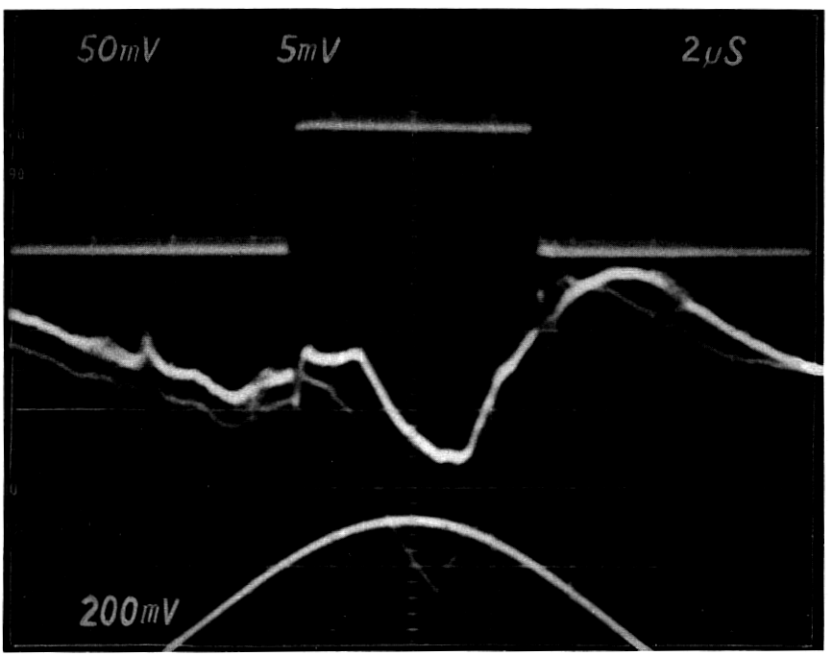

Fig. 30—Superimposed zero and one output waveforms of straight-bar detector at 2.5 mA and 55-Oe drive field intensity.

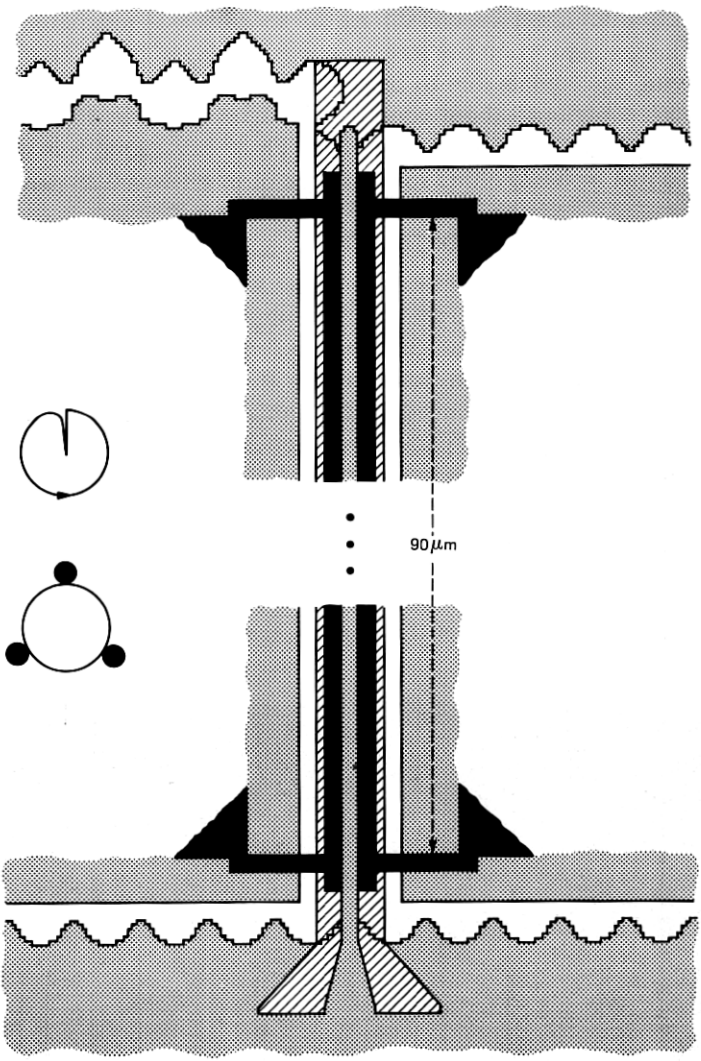

Fig. 31—Channel-bar detector using straight-bar Permalloy elements. The two bars serve as detector and reference detector, but both respond to the bubble, increasing the figure of merit.

of the bar switches. The 2 mV signal obtained at 2.5 mA into 325 ohms yielded a figure of merit of 0.25 percent.

XIV. CHIP ARCHITECTURE

Generally, the components described above support major-minor memory chip designs with provisions to save data being read or written during power interruptions. A good example is the closed G-loop

organization[14] shown schematically in Fig. 37a. Merge (M) and backward turns (B) were discussed, while the other propagate features are known from previous work. Read cycles are nonvolatile simply because the data are shifted around on a closed path. In write cycles, the new

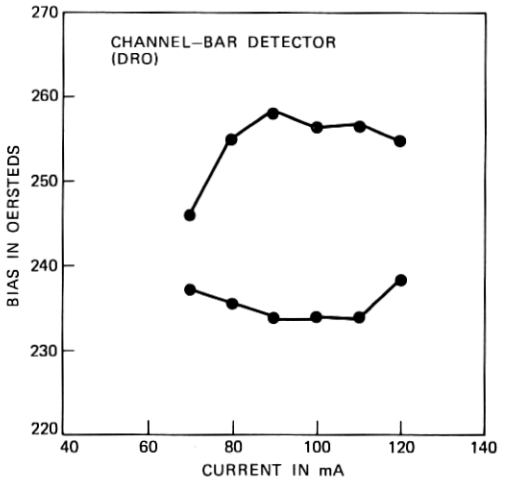

Fig. 32—Bias margins vs stretch and collapse current for channel-bar detector.

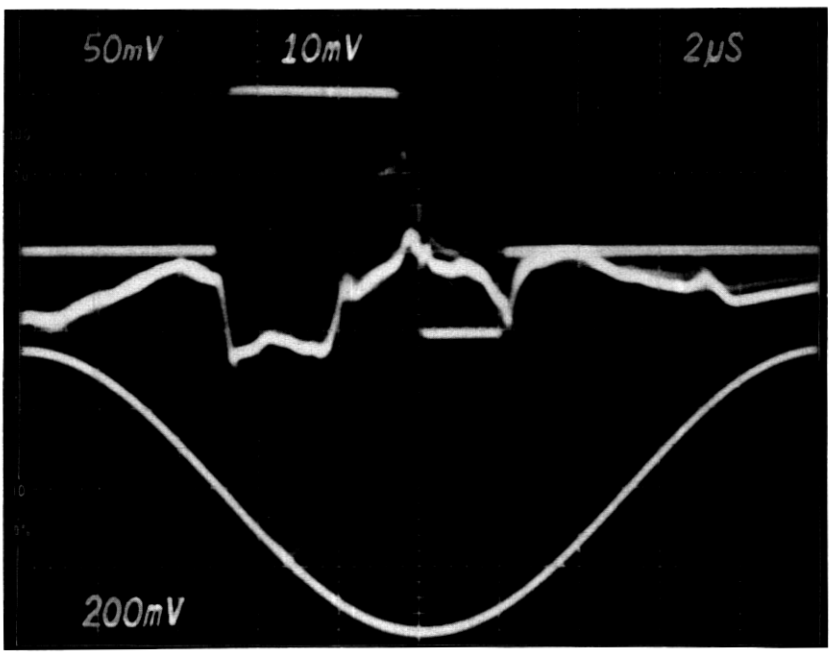

Fig. 33—Superimposed zero and one output waveforms for push-pull detector at 2.5 mA, and 40-Oe drive field with 5-Oe offset.

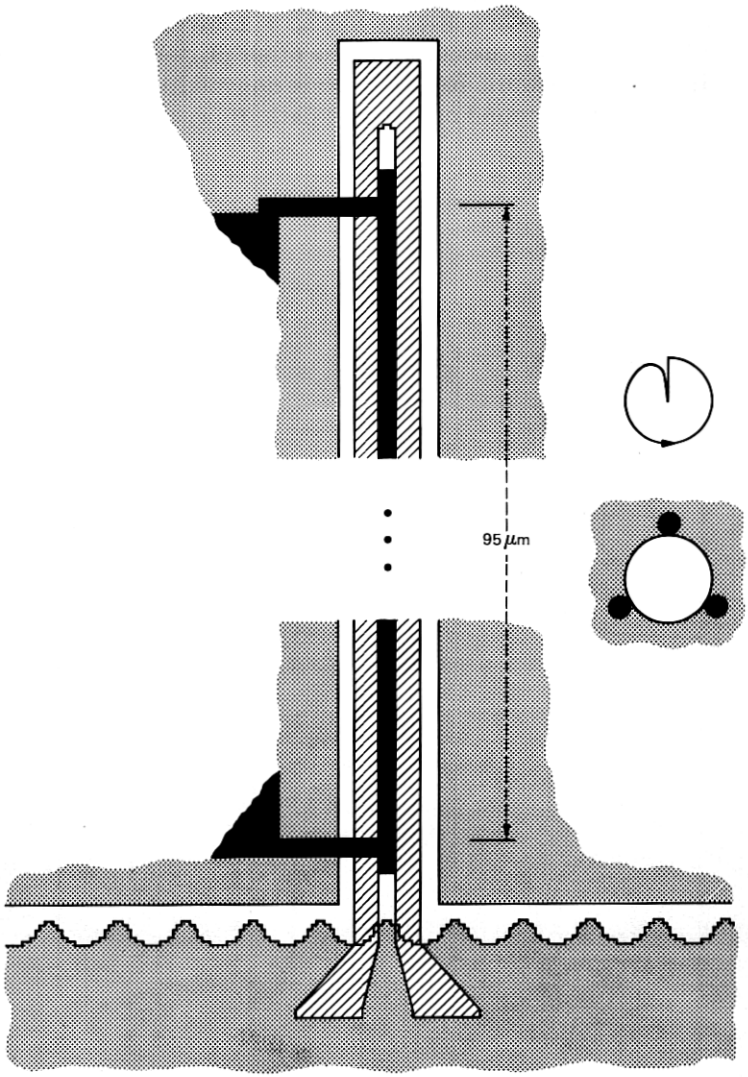

Fig. 34—Straight-bar detector over nominally unimplanted material.

data are written before the old are disturbed. A partially written block present after power restoration would be discarded. The capability to read data on every cycle is needed to accomplish block recognition on power restoration because blocks starting on both even and odd cycles may be present in the G-loop. The 2λ propagator described above could help detection on every cycle. Since it spaces the bubbles physically by the same distance as normally obtained with alternate-

cycle detection, they would be less likely to be collapsed by the detector's outside field during stretch pulses.

Another organization, shown in Fig. 37b, closes the path from the detector back to the write line electronically, with the help of the

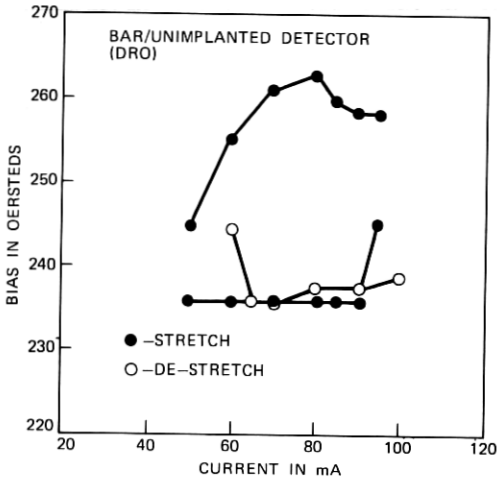

Fig. 35—Bias field margins vs current for straight-bar detector over unimplanted material.

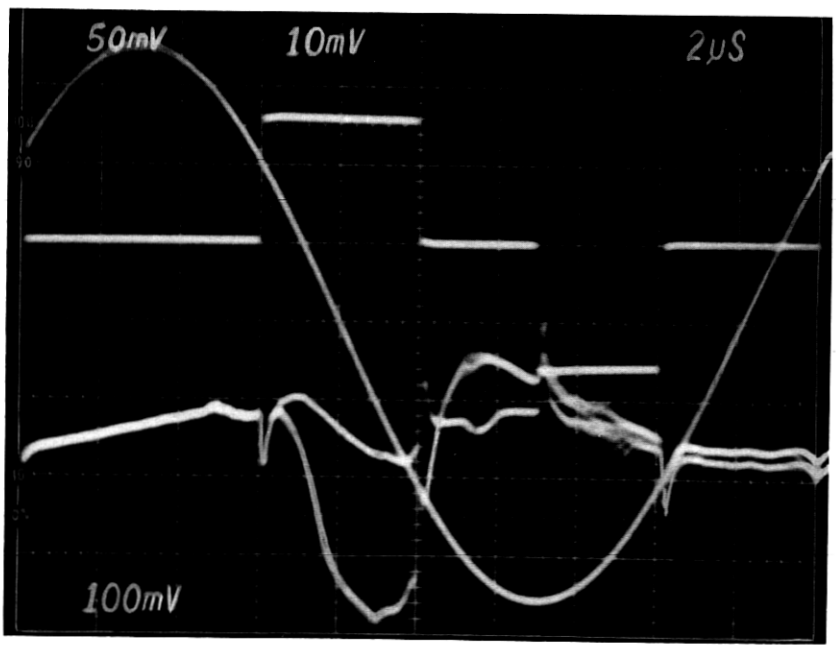

Fig. 36—Superimposed zero and one output waveforms for straight-bar detector over unimplanted material at 2.5 mA and 40-Oe drive field intensity.

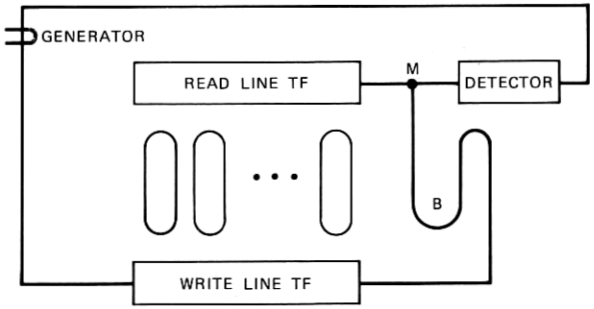

(a)

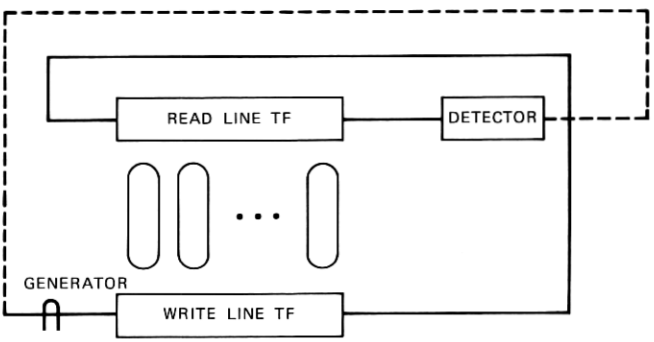

(b)

Fig. 37—Major-minor loop architecture assuming (a) nondestructive read-out and (b) destructive read-out of bubble-coded information.

generator. This organization appears to be attractive at this stage of the development of the device components because it uses only forward turns and because better margins are currently obtained with destructive read-out (DRO). If a power outage should occur during a read cycle, the data leaving the read line and entering the write line should be stopped on predetermined odd or even cycles with respect to the detector. This is needed if, as is likely, an alternate cycle detector is used which may mutilate data in intermediate cycles. With this provision, when power is restored, the system controller can complete the reading and rewriting of the block and circulate it once around the solid path to provide a complete read. This determines the block address of the data present. Finally, the data would be restored. Circulating the data around the two possible paths to the detector does not de-synchronize it with respect to the minor loops. The situation during a write cycle is similar, except that a partially altered block probably would be restored if power should be lost. A secure mode of writing, which increases the write cycle time, is possible. This write begins as in a read cycle, but the old information is permitted to

circulate around towards the detector while the new information is being written. At all times, either the old or the new information or both would be present in the closed path from the generator to the detector.

XV. CONCLUSIONS

The organization of Fig. 37b can be implemented with a subset of the device components described in this paper. Using the write-line transfer gate of Fig. 21 for transfer-in, the N-gate for transfer-out, and the unimplanted-bar detector shown in Fig. 34, over 20-Oe bias-field margins should be obtained at 40-Oe drive field. The organization in Fig. 37a should also operate over a 20-Oe bias range, using in addition the merge and backward turn propagate patterns. The channel-meander arrangement provides for nondestructive read-out, as required, but a less noisy Permalloy configuration is still needed in this case.

XVI. ACKNOWLEDGMENTS

We thank A. H. Bobeck, J. E. Geusic, C. J. Mogab, A. J. Perneski, and R. S. Wagner for helpful comments and suggestions. We also thank H. C. Alder and R. A. Keane for expert technical assistance.

REFERENCES

1. J. C. North, R. Wolfe and T. J. Nelson, "Applications of Ion Implantation to Magnetic Bubble Devices," J. Vac. Sci. Technology, *15* (1978), p. 1675.
2. T. J. Nelson and S. L. Blank, "Eight Micron Period Bubble Devices," IEEE Trans. Magnetics, *MAG-14* (1978), p. 1117.
3. S. L. Blank, R. Wolfe, L. C. Luther, R. C. LeCraw, T. J. Nelson, and W. A. Bidsi, "Design and Development of Single-Layer Ion-Implantable Small Bubble Materials for Magnetic Bubble Devices," J. Appl. Phys., *50* (1979), p. 2155.
4. T. J. Nelson, R. Wolfe, S. L. Blank and W. A. Johnson, "Reliable Propagation of Magnetic Bubbles with 8 μm Period Ion Implanted Propagation Patterns," J. Appl. Phys., *50* (1979), p. 2261.
5. R. Wolfe, J. C. North, W. A. Johnson, R. R. Spiwak, L. J. Varnerin, and R. F. Fischer, "Ion Implanted Patterns for Magnetic Bubble Propagation," AIP Conf. Proc., *10* (1972), p. 339.
6. Y. S. Lin, G. S. Almasi and G. E. Keefe, "Contiguous-Disk Bubble Domain Devices," IEEE Trans. Magnetics, *MAG-13* (1977), p. 1744.
7. Y. S. Lin, G. S. Almasi and G. E. Keefe, "Manipulation of 1 μm Bubbles with Coarse (>4 μm) Overlay Patterns," J. Appl. Phys., *48* (1977), p. 5201.
8. G. S. Almasi, G. E. Keefe and Y. S. Lin, "Nucleation of 1-μm Bubbles via Charged Walls," J. Appl. Phys. *50* (1979), p. 2273.
9. R. Wolfe and T. J. Nelson, "Crystal Symmetry Effects in Ion Implanted Propagation Patterns for Magnetic Bubbles—Roof-Top Designs," IEEE Trans. Magnetics, *MAG-15* (1979), p. 1323.
10. Y. S. Lin, G. S. Almasi, D. B. Dove, G. E. Keefe, and C. C. Shir, "Orientation Dependence of Propagation Margin of 1-μm Bubble Contiguous-Disk Devices—Clues and Cures," J. Appl. Phys., *50* (1979), p. 2258.
11. H. Jouve and I. Puchalska, "Some Characteristics of Ion-Implanted Bubble Chips," IEEE Trans. Magnetics, *MAG-15* (1979), p. 1016.
12. A. H. Bobeck, R. F. Fisher, A. J. Perneski, J. P. Remeika, and L. G. Van Uitert, "Application of Orthoferrites to Domain Wall Devices," IEEE Trans. Magnetics, *MAG-5* (1969), p. 544.
13. J. A. Copeland, J. G. Josenhans, and R. R. Spiwak," Circuit and Module Design for Conductor-Groove Bubble Memories," IEEE Trans. Magnetics, *MAG-9* (1973), p. 489.
14. T. M. Burford, unpublished work.